

## Mapping Time-course Mitochondrial Adaptations in the Kidney in Experimental Diabetes

Melinda T. Coughlan<sup>1,2,3</sup>, Tuong-Vi Nguyen<sup>1</sup>, Sally A. Penfold<sup>1</sup>, Gavin C. Higgins<sup>1,4</sup>,  
Vicki Thallas-Bonke<sup>1</sup>, Sih Min Tan<sup>1,2</sup>, Nicole J. Van Bergen<sup>5</sup>, Karly C. Sourris<sup>1,2</sup>,  
Brooke E. Harcourt<sup>6</sup>, David R. Thorburn<sup>6</sup>, Ian A. Trounce<sup>5</sup>, Mark E. Cooper<sup>1,2</sup>,  
Josephine M. Forbes<sup>1,7,8</sup>

<sup>1</sup>*Glycation, Nutrition & Metabolism Laboratory, Baker IDI Heart & Diabetes Institute, Melbourne, Victoria 8008, Australia.*

<sup>2</sup>*Department of Medicine, Central Clinical School, Monash University, Alfred Medical Research & Education Precinct, Melbourne 3004 Victoria, Australia.*

<sup>3</sup>*Department of Epidemiology & Preventive Medicine, Monash University, Alfred Medical Research & Education Precinct, Melbourne 3004, Victoria, Australia.*

<sup>4</sup>*Department of Biochemistry & Molecular Biology, Monash University, Clayton, 3800 Victoria, Australia.*

<sup>5</sup>*Centre for Eye Research Australia, Eye and Ear Hospital, East Melbourne, 3002 Victoria Australia.*

<sup>6</sup>*Murdoch Children's Research Institute, Royal Children's Hospital, Parkville 3052, Victoria, Australia.*

<sup>7</sup>*Glycation and Diabetes, Mater Research Institute-The University of Queensland, TRI, Woolloongabba, South Brisbane 4102, QLD, Australia.*

<sup>8</sup>*School of Medicine, Mater Clinical School, University of Queensland 4067, St Lucia, Australia.*

### Corresponding Author:

Melinda T. Coughlan  
Glycation, Nutrition & Metabolism Laboratory  
Baker IDI Heart & Diabetes Institute  
PO Box 6492, St Kilda Rd Central, Melbourne, 8008, Australia.  
Telephone: +61 3 8532 1278, Fax: +61 3 8532 1480  
Email: Melinda.Coughlan@bakeridi.edu.au

## **Abstract**

Oxidative phosphorylation drives ATP production by mitochondria, which are dynamic organelles, constantly fusing and dividing to maintain kidney homeostasis. In diabetic kidney disease, mitochondria appear dysfunctional, but the temporal development of diabetes-induced adaptations in mitochondrial structure and bioenergetics, have not been previously documented. Here, we map the changes in mitochondrial dynamics and function in rat kidney mitochondria at 4, 8, 16 and 32 weeks of diabetes. Our data reveal that changes in mitochondrial bioenergetics and dynamics precede the development of albuminuria and renal histological changes. Specifically, in early diabetes (4 weeks) a decrease in ATP content and mitochondrial fragmentation within proximal tubule epithelial cells of diabetic kidneys were clearly apparent, but no change urinary albumin excretion or glomerular morphology were evident at this time. By 8 weeks of diabetes, there was increased capacity for mitochondrial permeability transition (mPT) by pore opening, which persisted over time and correlated with mitochondrial hydrogen peroxide generation and glomerular damage. Late in diabetes, by week 16, tubular damage was evident with increased urinary Kidney injury molecule (Kim)-1 excretion, where an increase in Complex I-linked oxygen consumption rate, in the context of a decrease in kidney ATP, indicated mitochondrial uncoupling. Taken together, these data show that changes in mitochondrial bioenergetics and dynamics may precede the development of the renal lesion in diabetes, and this supports the hypothesis that mitochondrial dysfunction is a primary cause of diabetic kidney disease.

## **Summary statement**

We identified that dysfunction of cellular power stations, mitochondria, may precede the development of kidney disease in diabetes. This suggests that mitochondrial dysfunction is a primary cause of diabetic nephropathy, which could be targeted to improve the burden of this disease.

**Short title:** Mitochondrial adaptations in diabetic nephropathy

**Keywords:** mitochondria, diabetic nephropathy, experimental diabetes.

**Abbreviations list:**

ATP	adenosine triphosphate
CKD	chronic kidney disease
CsA	cyclosporin A
DKD	diabetic kidney disease
Drp-1	dynamain related protein-1
GSI	glomerulosclerotic index
H <sub>2</sub> O <sub>2</sub>	hydrogen peroxide
KIM-1	kidney injury molecule -1
Mff	mitochondrial fission factor
Mfn	mitofusin
MnSOD	manganese superoxide dismutase
mPT	mitochondrial permeability transition
mtDNA	mitochondrial DNA
nDNA	nuclear DNA
OCR	oxygen consumption rate
OPA-1	guanosine triphosphatase (GTPase) optic atrophy-1
OXPHOS	oxidative phosphorylation
PTEC	proximal tubular epithelial cell
ROS	reactive oxygen species

Accepted Manuscript

## Introduction

Chronic kidney disease (CKD) is a major risk factor for cardiovascular events and all-cause mortality (1), affecting more than 50 million individuals world-wide (2). CKD incidence is projected to dramatically increase over the next two decades, particularly in developing nations, as a result of key risk factors including hypertension, diabetes and associated cardiovascular disease (3). Hence, preventing the onset or progression of CKD is likely to significantly reduce all-cause mortality across many populations. At least 30-40% of the burden of CKD is as a result of diabetes (4), although not all diabetic individuals will develop kidney disease, suggesting that there is an underlying genetic predisposition to this disorder (5). Of the minority of patients with CKD who do not eventually die from a cardiovascular event, many will progress to end stage renal disease and require renal transplantation or dialysis. Along with management of hyperglycemia and hypertension, agents which target the renin angiotensin system are widely used in clinical practice in patients with diabetic kidney disease (DKD). Despite this, renal function still progressively declines in the majority of patients (6). Clearly, there is a critical need to identify the pathogenic factors that lead to the onset and progression from DKD to cardiovascular and end stage renal disease in order to develop novel therapeutic targets.

Mitochondria are fundamental to metabolic homeostasis by converting nutrient flux into ATP via the process of oxidative phosphorylation (OXPHOS). Normal kidney function is energetically demanding and the proximal tubule of the kidney generates vast quantities of ATP via OXPHOS to facilitate active reabsorption of macromolecules (7). Many lines of evidence suggest that mitochondrial dysfunction and bioenergetic defects play a central role in the development of DKD (8-15) with mitochondrial ATP depletion and mitochondrial uncoupling features of disrupted mitochondrial homeostasis. A clear link between DKD and a shift in mitochondrial dynamics has also recently emerged from studies demonstrating mitochondrial fragmentation in the diabetic kidney (16-18), however, whether these changes in mitochondrial dynamics and bioenergetics are present prior to the development of early renal structural and biochemical lesions remains unknown.

To address this issue, we used a streptozotocin-induced diabetic rat model, which allowed us to study early changes in the kidney that are difficult to map in individuals with diabetes. This well-established model of diabetes complications has most hallmarks of progressive human DKD including hyperfiltration, albuminuria and renal structural defects. Hence we could study temporal changes in renal function and morphology and link these to adaptive mechanisms in mitochondria, in particular mitochondrial function and structure.

## Research Design and Methods

### ***Experimental Animal Model***

All animal experiments were performed in accordance with guidelines from the Alfred Medical Research and Education Precinct Animal Ethics Committee and the National Health and Medical Research Council of Australia. Animals were housed in groups of three rats per cage in a temperature-controlled environment, with a 12 h light/dark cycle and *ad libitum* access to food and water. Experimental diabetes was induced in six week old male Sprague Dawley rats (200-250g) by *i.v.* injection of streptozocin (50mg/kg, sodium citrate buffer pH 4.5) following an overnight fast (19). Animals with plasma glucose concentrations in excess of 15 mmol/l, one-week post induction of diabetes were included in the study. Diabetic and control animals were randomised into groups ( $n=10$  per group) and followed for either 4, 8 weeks, 16 or 32 weeks. Two to three units of insulin (Humalog, Eli-Lilly, Indianapolis, USA) were administered daily to diabetic animals to prevent ketoacidosis and improve survival. Twenty four-hours before the study time-points, rats were placed individually into metabolic cages (Iffa Credo, L'Arbresle, France). Blood glucose was measured using a glucometer (Accutrend; Boehringer Mannheim Biochemica, Mannheim, Germany). Glycated haemoglobin (GHb) was determined by a Cobas Integra 400 autoanalyzer (Roche Diagnostics Corporation, USA). At the specified time-points, animals were euthanased and the kidneys were rapidly dissected, weighed, and snap-frozen or placed in 10% neutral buffered formalin (v/v) for fixation before paraffin embedding. In a subset of rats ( $n=5$  per group), mitochondria were isolated from fresh renal cortices as later described. Renal cortices from five rats per group were processed for transmission electron microscopy as described below.

### ***Renal Function and Morphometry***

Rat-specific ELISAs were used to measure urinary albumin excretion (Bethyl Laboratories, Montgomery, TX, USA), urinary Kidney Injury Molecule-1 (KIM-1, USCN Life Sciences, Wuhan, China) and serum Cystatin C (BioVendor, Mordice, Czech Republic) as per the manufacturer's specifications. Glomerulosclerotic index (GSI) was assessed in Periodic Acid Schiff (PAS)-stained sections as previously described (20).

### ***Transmission electron microscopy and analysis of mitochondrial morphology***

Immediately following exsanguination, renal cortices were fixed in 2.5% glutaraldehyde in PBS buffer for four hours at room temperature. The samples were then rinsed three times in fresh buffer for 15 minutes each before post-fixing in 1% osmium tetroxide in buffer for 2 hours at room temperature. Fixed tissue samples were rinsed three times in fresh buffer for ten minutes each, before being dehydrated in increasing concentrations of ethanol consisting of 10, 30, 50, 70, 90, 100 and 100 % anhydrous ethanol for 60 minutes each step. Following dehydration the cells were infiltrated with increasing concentrations of LR White resin in ethanol consisting of 25, 50, 75 and 100 % resin for six hours each step. After a second change of 100 % resin the samples were embedded in fresh resin in gelatine capsules and allowed to

sink to the bottom. The gelatine capsules were capped to exclude air and the resin polymerised in an oven at 60°C for 24 hours. The embedded tissues in resin blocks were sectioned with a diamond knife on a Leica Ultracut S microtome and ultra-thin sections (90 nm) were collected onto formvar-coated 100 mesh hexagonal copper grids. The sections on grids were sequentially stained with 1% uranyl acetate for 10 mins and Triple Lead Stain for 5 min (21) and viewed in a Phillips CM120 Biotwin transmission electron microscope at 120 kV. Images were captured with a Gatan Multiscan 600CW digital camera at a resolution of 1024 x 1024 pixels. Ten images of proximal tubule epithelial cells per kidney section were randomly collected for each rat ( $n=5$  rats per group) at x15,000 magnification. Mitochondrial length and width of all mitochondria within a given image (from 10 images per rat) were measured using ImageJ (National Institutes of Health, Bethesda, MD, USA) and the aspect ratio calculated (length/width) and expressed as mean aspect ratio per group. In addition, mitochondrial roundness was evaluated using ImageJ within each field per section and expressed as mean mitochondrial roundness per group.

### ***Mitochondrial isolation***

Mitochondria from fresh rat kidneys were isolated from 100 mg of renal cortex by differential centrifugation as previously described (22).

### ***ATP***

Mitochondrial ATP was measured using a bioluminescence ATP determination kit (Molecular Probes, Life Technologies, Melbourne, Australia) as described previously (23, 24) with the following modifications. A ten-point standard curve was prepared, ranging from 50,000 nM to 125nM. Data were normalized to citrate synthase activity and percentage control at the same time-point.

### ***Citrate Synthase activity***

Citrate synthase activity was assayed as previously described (22).

### ***Oxygen consumption rate***

Oxygen consumption rates in isolated mitochondria from control and diabetic rats were measured using an Oxygraph-2 k high resolution respirometer (Oroboros Instruments, Innsbruck Austria) (25).

### ***Mitochondrial permeability transition***

The induction of mitochondrial permeability transition (mPT) in rat kidney mitochondria was monitored by absorbance changes at 540 nm based on a microtiter plate procedure developed by Waldmeier et al (26), with the following modifications. Rat kidney cortex obtained 10 min after euthanasia was homogenised in 5 mM HEPES containing 1 mM EGTA, 210 mM mannitol, and 70 mM sucrose, pH 7.2. Mitochondria were isolated by differential centrifugation, washed twice and resuspended in energised respiratory buffer (210 mM mannitol, 70 mM sucrose, 5 mM glutamate, 5 mM malate, 0.05 M Tris, 5 mM H<sub>3</sub>PO<sub>4</sub>, pH 7.4). Mitochondrial protein, 1 mg, was added to each well along with 82  $\mu$ l energised respiratory buffer



and 10  $\mu$ M Cyclosporin A (CsA) where appropriate. Five min after the addition of CsA, 200  $\mu$ M  $\text{CaCl}_2 \cdot 2\text{H}_2\text{O}$  was added and the absorbance over 10 min was determined using a Wallac 1420 Victor<sup>3</sup> V Multilabel Counter (Perkin Elmer, Wellesley, MA, USA).

### ***Mitochondrial hydrogen peroxide production***

Hydrogen peroxide production was measured in isolated mitochondria using the Amplex Red reagent as previously described (22).

### ***Superoxide dismutase activity***

The activity of superoxide dismutase in isolated mitochondria was assayed using the Cayman Chemical Company assay kit (Ann Arbor, MI, USA) according to the manufacturer's instructions. Briefly, 10  $\mu$ l of mitochondrial or cytosolic isolate, or standard in duplicate was added to 200  $\mu$ l of radical detector. The reaction was initiated by 20  $\mu$ l xanthine oxidase, incubated for 20 min at room temperature and the SOD activity was measured at 450 nm. Enzymatic activity was expressed as mU per mg of total protein.

### ***15-isoprostane $F_{2t}$ ELISA***

Urinary isoprostane excretion (15-isoprostane  $F_{2t}$ ) was measured by a competitive ELISA specifically designed for urine (Oxford Biomedical Research, Oxford MI), according to the manufacturer's instructions.

### ***Western Immunoblotting***

Renal cortices were homogenised using a Next Advance Bullet Blender 24 (Averill Park, NY, USA) at 4°C, with 1.00 and 2.00 mm beads at speed 8 for 4 min in RIPA extraction buffer (10 mM Tris-HCl pH 8.0, 150 mM NaCl, 1% NP-40, 1% sodium deoxycholate, 0.1% SDS), containing Protease Inhibitor Cocktail (Roche, Castle Hill, NSW, Australia) and Phosphatase Inhibitor Cocktail 2 (Sigma-Aldrich Pty Ltd, Sydney, Australia). The supernatant was obtained following centrifugation (15,000 x g, 15 min) at 4°C and protein content determined using a BCA Protein Assay Kit (Pierce-Thermo Fisher Scientific, Melbourne, Australia). Immunoblotting was performed using  $\beta$ -actin (AC-15; 1:10,000) (Abcam, Melbourne, Vic, Australia) and rat monoclonal anti-OPA1 (1:1,000, BD Transduction Laboratories, North Ryde, Australia).

### ***Quantitative Reverse Transcription-Polymerase Chain Reaction (qRT-PCR)***

RNA was isolated from kidney cortex (20-30 mg) using TRIzol Reagent (Life Technologies). DNA-free RNA was reverse transcribed into cDNA using the Superscript First Strand Synthesis System according to the manufacturer's specifications (Life Technologies BRL, Grand Island, NY). Real-time PCR was performed using SYBR green PCR mix (Applied Biosystems, primer concentration of

500 nM) using a 7500 Fast Real-time PCR System (Applied Biosystem, VIC, Australia), and normalized relative to the 18S ribosomal RNA.

### ***mtDNA copy number***

DNA was extracted from renal cortex using a Maxwell 16 Instrument (Promega). DNA concentration was determined using a NanoDrop 1000 (Thermo Scientific). Mitochondrial DNA (mtDNA) copy number was determined by comparing the ratio of mtDNA to nuclear DNA (nDNA). Taqman primers and probes for POP5 (Processing of Precursor 5 gene; Rn02108253\_s1, VIC-MGB, Applied Biosystems) was used as the nDNA reference gene. MT-CO3 (Mitochondrially Encoded Cytochrome C Oxidase III; Rn03296820\_s1, FAM-MGB, Applied Biosystems) was used as the mtDNA reference gene. SDHA (Succinate Dehydrogenase Complex, Subunit A; Custom Ref #CCRR90D, NED-MGB, Applied Biosystems) a mitochondrial, nuclear coded gene (mt(nDNA)) was used as an internal control. The three Taqman probes were multiplexed using a standard PCR run with TaqMan Master Mix (Applied Biosystems) and run on a 386-well QuantStudio 7 Flex System, Applied Biosystems. The ratio of mtDNA/nDNA and mt(nDNA)/nDNA was determined by comparing CT values for each gene. PCR settings were denaturation at 95°C for 10 mins, x40 cycles of annealing at 95°C for 15 secs and extension at 60°C for 1 min. Genomic

### ***Statistics***

All statistical computations were performed using GraphPad Prism version 6.0 for Mac OS X (GraphPad Software, San Diego, California, USA). Values of experimental groups are given as mean, with bars showing the SEM, unless otherwise stated. Time and disease status (diabetes) effects were tested using Two-way ANOVA with Bonferroni post-hoc analysis. A  $P < 0.05$  was considered to be statistically significant.

## **Results**

### ***Time-course of diabetic kidney disease.***

Body weight was decreased in diabetic rats compared to control rats at each timepoint (Table 1). Kidney to body weight ratio, blood glucose and glycated hemoglobin (GHb) were each increased in diabetic animals compared to control within each time-point. Serum cystatin C, as a marker for glomerular filtration rate (Figure 1A) was decreased as early as 4 weeks after diabetes was established, indicating renal hyperfiltration, consistent with individuals with diabetes. Albuminuria had developed by 16 weeks of diabetes (Figure 1B) and this was preceded by glomerular morphological changes, glomerulosclerosis, which was apparent by week 8 of diabetes (Figure 1C&D). Significant tubular damage was evident by late diabetes (32 weeks) as reflected by an increase in urinary excretion of Kidney Injury Molecule (Kim)-1 (Figure 1E).

### ***Changes in mitochondrial bioenergetics precede development of renal structural injury and albuminuria.***



Mitochondrial bioenergetics were measured in freshly isolated mitochondria from kidney tissue (renal cortices). At 4 weeks of diabetes, mitochondrial ATP content was significantly decreased compared to control kidney, which persisted to 8 and 32 weeks of diabetes (Figure 2A). Although unchanged at weeks 4 and 8, mitochondrial respiration, assessed by oxygen consumption rate (OCR) during both State III and uncoupled respiration in the presence of Complex I substrates glutamate and malate was increased at weeks 16 and 32 in diabetic kidneys (Figure 2&C).

***Enhanced susceptibility to mitochondrial permeability transition pore opening coincides with the development of renal morphological lesions.***

Freshly isolated mitochondria from renal cortices were exposed to vehicle, calcium (to induce pore opening) or calcium plus the mPT pore inhibitor, cyclosporin A, and mPT pore opening (swelling) was assessed by light scattering at 450 nm. Four weeks after the development of diabetes, there was no change in mPT pore opening (Figure 3A). By 8 weeks of diabetes, there was an increased capacity for calcium-induced mPT pore opening, which persisted over the diabetes time-course (Figure 3B-D). mPT pore opening was inhibited by CsA, an inhibitor of mPT (Figure 3D).

***Both early and late diabetes are characterized by mitochondrial fragmentation.***

Next we explored mitochondrial morphology within proximal tubule epithelial cells (PTECs), which constitute ~90% of the kidney cortex. Transmission electron microscopy showed mitochondria of a mixed population in PTECs in 4 and 32 week control kidney sections (Figure 4A, left), that is, fragmented, intermediate and elongated. However, mitochondria in PTECs of diabetic rats were more fragmented (Figure 4A, right), both at 4 and 32 weeks of diabetes. This fragmented appearance was confirmed by assessment of mitochondrial aspect ratio, which takes into account both length and width, which was also decreased by diabetes at both time-points (Figure 4B). Mitochondrial roundness was also increased in the context of diabetes, further confirming a more fragmented phenotype in the diabetic kidney sections (Figure 4C).

***Proteins involved in mitochondrial fission and fusion are altered throughout the time-course of diabetes in the kidney.***

Western immunoblotting of the protein guanosine triphosphatase (GTPase) optic atrophy (OPA)-1 demonstrated that the Long isoform 1 and 2 (L1 and L2) and three short isoforms (S1, S2 and S3) (27) were detected in both control and diabetic kidneys (Figure 5A-F). The abundance of fusion-associated L1 and L2 were increased at 4 weeks of diabetes (Figure 5A&B), whilst only L1 was decreased at 32 weeks of diabetes (Figure 5A). The short isoforms are thought to regulate mitochondrial fission. There was no change in S1 (Figure 5C), but S2 was increased at week 16 (Figure 5D) and S3 by at 32 weeks of diabetes (Figure 5E). The gene expression of both Mitofusin-1 (*Mfn1*) and mitofusin-2 (*Mfn2*), which regulate outer mitochondrial membrane fusion (28), were increased in the renal cortex of diabetic rats at 4 weeks of diabetes (Figure 5G&H respectively). Mitochondrial fission factor (*Mff*) expression was also up-regulated in early diabetes (Figure 5I).

***The oxidative stress response is an early change in the diabetic kidney.***

Mitochondrial hydrogen peroxide production was increased at weeks 8, 16 and 32 of diabetes (Figure 6A). Manganese superoxide dismutase activity (MnSOD), a key mitochondrial antioxidant enzyme was suppressed from week 4 after diabetes and throughout diabetes duration (Figure 6B). Urinary excretion of 15-isoprostane F<sub>2t</sub>, a marker of lipid peroxidation was also increased early in diabetes, indicating an overall increase in oxidative stress status (Figure 6C).

***Mitochondrial DNA copy number is increased in early diabetes.***

The ratio of mitochondrial (mt)-DNA to nuclear (n)-DNA was increased in the diabetic kidney at week 4 after diabetes (C,  $0.75 \pm 0.02$  vs D,  $0.78 \pm 0.01$ ;  $P=0.012$ ), but this did not persist to week 8, 16 or 32, with no affect over time on mtDNA copy number in either control rats nor those with diabetes.

Accepted Manuscript

## Discussion

The present study has demonstrated that changes in mitochondrial bioenergetics and structure occur precede the development of albuminuria and renal structural defects in diabetes. As early as four weeks after diabetes induction, the ATP content within kidney mitochondria had decreased, and this was accompanied by the fragmentation of mitochondria, the increased expression of mitochondrial networking regulators OPA-1 long isoforms, *Mfn1/2* and *Mff*, and an increase in mtDNA copy number and kidney hyperfiltration. Mitochondrial fragmentation was also associated with an increase in reactive oxygen species (ROS) generation. These mitochondrial defects persisted and by 16 weeks, when albuminuria and structural abnormalities had developed, there was evidence of a compensatory shift in State III and in uncoupled ATP production and mitochondrial dynamics, which restored kidney ATP content. However, by week 32 of diabetes, these compensatory mechanisms were not adequate to maintain kidney ATP concentrations, which were significantly decreased in line with the onset of tubular damage, marked by the increase in urinary Kim-1. Taken together, these data allude to mitochondrial abnormalities being primary initiators of diabetic kidney disease.

The kidneys are highly dependent on aerobic ATP production by OXPHOS in mitochondria (7) and at rest consume 7% of the body's molecular oxygen (29). Consistent with the present study, there is previous evidence that sustained hyperglycaemia results in increased kidney oxygen consumption, attributed to mitochondrial dysfunction (30). In general however, these studies show increased kidney oxygen consumption later in the progression of diabetic nephropathy, resulting in intra-renal tissue hypoxia, likely the result of an imbalance between increased oxygen consumption and delivery, leading to kidney fibrosis (30). Interestingly, early kidney hyperfiltration at week 4 of the study may have increased oxygen delivery with diabetes and this was sustained for the duration of the study. We have also previously shown that a genetic mutation in the respiratory chain inducing mitochondrial dysfunction, results in a decrease in kidney ATP content in the context of increased oxygen consumption and renal disease in adult mouse kidneys (22).

It has remained unclear, however, as to why in diabetes, the mitochondria are dysfunctional before oxygen consumption increases in the kidney. Indeed, in the present study, a decrease in kidney cortical ATP content was already evident by 4 weeks of diabetes, in the absence of increased mitochondrial oxygen consumption. Mitochondrial structure was also changed early in the development of diabetic kidney disease in our model, whereby mitochondria were fragmented and rounded at four weeks of diabetes. Fragmentation of mitochondria is a hallmark of ATP deficiency (31), in agreement with the decline in mitochondrial ATP content at the 4 week time-point of diabetes in the present study. There are other disorders where mitochondrial fragmentation and ATP loss are seen, such as in Huntington's disease where the early administration of agents that inhibit mitochondrial fission prevent tissue damage (32). Similarly, inhibition of mitochondrial fission by overexpressing a fission

mutant (DLP1-K38A) protects against diabetes-induced mitochondrial fission in proximal tubule cells and improves renal function (17).

The expression of key proteins involved in mitochondrial networking were also altered by 4 weeks of diabetes in the kidney. This included molecules associated with fission, *Mff*, as well as fusion, OPA1 long isoforms, *Mff1 and 2*. However, given that EM analysis clearly revealed that mitochondrial fragmentation was present, mitochondrial fission was the predominating mitochondrial structural phenotype in early diabetes. It is puzzling as to why the fission phenotype has persisted in the kidney throughout the duration of the disease, despite, in general, a variation of mitochondrial networking molecules. This suggests that the drive for restoration of ATP content may be a more important signal for mitochondrial fission, rather than the fission of mitochondria driving ATP deficit *per se*. It should be noted that mtDNA copy number was increased in early diabetes, suggesting induction of mitochondrial biogenesis at this time-point, but this was not sustained throughout diabetes duration. In our study, the reasons for sustained mitochondrial fragmentation in the kidney remain unclear. However, it is possible that there is regulation of fission by other proteins which regulate mitochondrial dynamics such as Parkin (33), and this may be driven by the search for alternative fuel sources (34). Certainly, this is an area of great interest currently and warrants further investigation in diabetic kidney disease.

There was also a sustained increase in the generation of renal cortical hydrogen peroxide from mitochondria from rats with diabetes, which could have been responsible for the mitochondrial fragmentation observed in the PTECs. Indeed, imbalances in mitochondrial ROS production are a recognized stimulus for mitochondrial fragmentation (33). It is also conceivable that the increases in ROS leading to mitochondrial fragmentation, are the result of increases in NADPH oxidase activity which are characteristic of the diabetic kidney (9), although this was not assessed in the present study. Diabetes-induced increases in the generation of hydrogen peroxide have also been shown to lead to mPT opening (8) as seen in the present study. It is likely that the increase in mPT i.e., opening of the mPT pore, could also contribute to the decrease in ATP content observed in the diabetic kidneys, since it is a trafficking site for ADP and ATP between the cytosol and mitochondria. Further, the mPT opening was induced in the presence of calcium which is a stimulus known to be altered in the diabetic milieu (33) by processes such as endoplasmic reticulum stress.

Overall, this group of studies postulates that defects in mitochondrial function are primary initiators of kidney disease in diabetes. Mitochondrial fragmentation and ATP loss were seen with diabetes before evidence of renal injury was present. Further, the evidence indicates that excess ROS generation and increased susceptibility to mPT were more tightly linked to the changes in mitochondrial morphology and function, rather than sustained changes in typical mitochondrial networking proteins. Hence, kidney function in diabetes may be improved by strategies to prevent mitochondrial dysfunction and this should be an area of prioritized research effort in the future for this disease.

### **Acknowledgments**

The authors would like to thank Amy Morley, Felicia Yap, Anna Gasser and Maryann Arnstein for their technical expertise. We would also like to thank Dr Simon Crawford (University of Melbourne) for assistance with electron microscopy.

### **Declarations of interest**

The authors have nothing to disclose.

### **Funding information**

This work was completed with support from the Juvenile Diabetes Research Foundation (JDRF), the National Health and Medical Research Council of Australia (NHMRC), the Mater Foundation and the Victorian Government's Operational Infrastructure Support Program. MTC is supported by the Australian and New Zealand Society of Nephrology Career Development Fellowship. GCH is supported by a postdoctoral fellowship from JDRF. JMF, DRT and MEC are NHMRC Research Fellows. Darren Henstridge has been supported by a Postdoctoral Fellowship from the National Heart Foundation of Australia and the Australian Diabetes Society. The authors have no conflicting financial interests.

### **Author contribution statement**

MTC ran the animal studies, researched the data and co-wrote the paper. TVN, SAP, GCH, VTB, SMT, NJVB, KCS, BEH, DRT, IAT and MEC researched the data. JMF conceived the studies, researched the data and co-wrote the paper.

### **Clinical perspectives**

- Mitochondrial dysfunction is seen at sites of diabetes complications including in the kidneys.
- We hypothesized that mitochondrial dysfunction is an early event in the pathogenesis of diabetic kidney disease.
- This study showed that mitochondrial dysfunction precedes kidney dysfunction in diabetes and hence may be a primary cause of diabetic nephropathy able to be therapeutically targeted to prevent this disease.



## References

1. Go AS, Chertow GM, Fan D, McCulloch CE, Hsu CY. Chronic kidney disease and the risks of death, cardiovascular events, and hospitalization. *N Engl J Med*. 2004 Sep 23;351(13):1296-305. PubMed PMID: 15385656. Epub 2004/09/24. eng.
2. Lysaght MJ. Maintenance dialysis population dynamics: current trends and long-term implications. *J Am Soc Nephrol*. 2002 Jan;13 Suppl 1:S37-40. PubMed PMID: 11792760. Epub 2002/01/17. eng.
3. Couser WG, Remuzzi G, Mendis S, Tonelli M. The contribution of chronic kidney disease to the global burden of major noncommunicable diseases. *Kidney Int*. 2011 Dec;80(12):1258-70. PubMed PMID: 21993585. Epub 2011/10/14. eng.
4. Collins AJ, Foley RN, Herzog C, Chavers B, Gilbertson D, Ishani A, et al. United States Renal Data System 2008 Annual Data Report. *Am J Kidney Dis*. 2009 Jan;53(1 Suppl):S1-374. PubMed PMID: 19111206. Epub 2009/01/15. eng.
5. Palmer ND, Freedman BI. Insights into the genetic architecture of diabetic nephropathy. *Curr Diab Rep*. 2012 Aug;12(4):423-31. PubMed PMID: 22573336. Pubmed Central PMCID: 3389140. Epub 2012/05/11. eng.
6. Brenner BM, Cooper ME, de Zeeuw D, Keane WF, Mitch WE, Parving HH, et al. Effects of losartan on renal and cardiovascular outcomes in patients with type 2 diabetes and nephropathy. *N Engl J Med*. 2001 Sep 20;345(12):861-9. PubMed PMID: 11565518. Epub 2001/09/22. eng.
7. Soltoff SP. ATP and the regulation of renal cell function. *Annual review of physiology*. 1986;48:9-31. PubMed PMID: 3010834. Epub 1986/01/01. eng.
8. Coughlan MT, Thorburn DR, Penfold SA, Laskowski A, Harcourt BE, Sourris KC, et al. RAGE-induced cytosolic ROS promote mitochondrial superoxide generation in diabetes. *J Am Soc Nephrol*. 2009 Apr;20(4):742-52. PubMed PMID: 19158353. Pubmed Central PMCID: 2663823. Epub 2009/01/23. eng.
9. Forbes JM, Coughlan MT, Cooper ME. Oxidative stress as a major culprit in kidney disease in diabetes. *Diabetes*. 2008 Jun;57(6):1446-54. PubMed PMID: 18511445. Epub 2008/05/31. eng.
10. Sharma K, Karl B, Mathew AV, Gangoiti JA, Wassel CL, Saito R, et al. Metabolomics reveals signature of mitochondrial dysfunction in diabetic kidney disease. *J Am Soc Nephrol*. 2013 Nov;24(11):1901-12. PubMed PMID: 23949796. Pubmed Central PMCID: 3810086. Epub 2013/08/21. eng.
11. Sivitz WI, Yorek MA. Mitochondrial dysfunction in diabetes: from molecular mechanisms to functional significance and therapeutic opportunities. *Antioxidants & redox signaling*. 2010 Apr;12(4):537-77. PubMed PMID: 19650713. Pubmed Central PMCID: 2824521. Epub 2009/08/05. eng.
12. Daehn I, Casalena G, Zhang T, Shi S, Fenninger F, Barasch N, et al. Endothelial mitochondrial oxidative stress determines podocyte depletion in segmental glomerulosclerosis. *J Clin Invest*. 2014 Apr 1;124(4):1608-21. PubMed PMID: 24590287. Pubmed Central PMCID: 3973074. Epub 2014/03/05. eng.
13. Che R, Yuan Y, Huang S, Zhang A. Mitochondrial dysfunction in the pathophysiology of renal diseases. *Am J Physiol Renal Physiol*. 2014 Feb 15;306(4):F367-78. PubMed PMID: 24305473. Epub 2013/12/07. eng.
14. Hall AM, Unwin RJ. The not so 'mighty chondrion': emergence of renal diseases due to mitochondrial dysfunction. *Nephron Physiol*. 2007;105(1):p1-10. PubMed PMID: 17095876. Epub 2006/11/11. eng.



15. Rosca MG, Mustata TG, Kinter MT, Ozdemir AM, Kern TS, Szweda LI, et al. Glycation of mitochondrial proteins from diabetic rat kidney is associated with excess superoxide formation. *American journal of physiology Renal physiology*. 2005 Aug;289(2):F420-30. PubMed PMID: 15814529.
16. Wang W, Wang Y, Long J, Wang J, Haudek SB, Overbeek P, et al. Mitochondrial fission triggered by hyperglycemia is mediated by ROCK1 activation in podocytes and endothelial cells. *Cell Metab*. 2012 Feb 8;15(2):186-200. PubMed PMID: 22326220. Pubmed Central PMCID: 3278719. Epub 2012/02/14. eng.
17. Galloway CA, Lee H, Nejjar S, Jhun BS, Yu T, Hsu W, et al. Transgenic control of mitochondrial fission induces mitochondrial uncoupling and relieves diabetic oxidative stress. *Diabetes*. 2012 Aug;61(8):2093-104. PubMed PMID: 22698920. Pubmed Central PMCID: 3402299. Epub 2012/06/16. eng.
18. Zhan M, Usman IM, Sun L, Kanwar YS. Disruption of Renal Tubular Mitochondrial Quality Control by Myo-Inositol Oxygenase in Diabetic Kidney Disease. *J Am Soc Nephrol*. 2014 Sep 30. PubMed PMID: 25270067. Epub 2014/10/02. Eng.
19. Coughlan MT, Forbes JM. Temporal increases in urinary carboxymethyllysine correlate with albuminuria development in diabetes. *American journal of nephrology*. 2011;34(1):9-17. PubMed PMID: 21654162.
20. Saito T, Sumithran E, Glasgow EF, Atkins RC. The enhancement of aminonucleoside nephrosis by the co-administration of protamine. *Kidney Int*. 1987 Nov;32(5):691-9. PubMed PMID: 3323599. Epub 1987/11/01. eng.
21. Sato T. A modified method for lead staining of thin sections. *Journal of electron microscopy*. 1968;17(2):158-9. PubMed PMID: 4177281.
22. Forbes JM, Ke BX, Nguyen TV, Henstridge DC, Penfold SA, Laskowski A, et al. Deficiency in Mitochondrial Complex I Activity Due to Ndufs6 Gene Trap Insertion Induces Renal Disease. *Antioxidants & redox signaling*. 2013 Mar 1;19(4):331-43. PubMed PMID: 23320803. Epub 2013/01/17. Eng.
23. Coughlan MT, Yap FY, Tong DC, Andrikopoulos S, Gasser A, Thallas-Bonke V, et al. Advanced glycation end products are direct modulators of beta-cell function. *Diabetes*. 2011 Oct;60(10):2523-32. PubMed PMID: 21911745. Pubmed Central PMCID: 3178291. Epub 2011/09/14. eng.
24. Drew B, Leeuwenburgh C. Method for measuring ATP production in isolated mitochondria: ATP production in brain and liver mitochondria of Fischer-344 rats with age and caloric restriction. *Am J Physiol Regul Integr Comp Physiol*. 2003 Nov;285(5):R1259-67. PubMed PMID: 12855419.
25. Lee S, Sheck L, Crowston JG, Van Bergen NJ, O'Neill EC, O'Hare F, et al. Impaired complex-I-linked respiration and ATP synthesis in primary open-angle glaucoma patient lymphoblasts. *Investigative ophthalmology & visual science*. 2012 Apr;53(4):2431-7. PubMed PMID: 22427588.
26. Waldmeier PC, Feldtrauer JJ, Qian T, Lemasters JJ. Inhibition of the mitochondrial permeability transition by the nonimmunosuppressive cyclosporin derivative NIM811. *Molecular pharmacology*. 2002 Jul;62(1):22-9. PubMed PMID: 12065751.
27. Anand R, Wai T, Baker MJ, Kladt N, Schauss AC, Rugarli E, et al. The i-AAA protease YME1L and OMA1 cleave OPA1 to balance mitochondrial fusion and

- fission. *J Cell Biol.* 2014 Mar 17;204(6):919-29. PubMed PMID: 24616225. Pubmed Central PMCID: 3998800. Epub 2014/03/13. eng.
28. Westermann B. Mitochondrial fusion and fission in cell life and death. *Nat Rev Mol Cell Biol.* 2010 Dec;11(12):872-84. PubMed PMID: 21102612. Epub 2010/11/26. eng.
29. Valtin H. *Renal Function: Mechanisms Preserving Fluid and Solute Balance in Health.* 2nd Edition. ed. Boston: Little Brown; 1983.
30. Friederich-Persson M, Thorn E, Hansell P, Nangaku M, Levin M, Palm F. Kidney hypoxia, attributable to increased oxygen consumption, induces nephropathy independently of hyperglycemia and oxidative stress. *Hypertension.* 2013 Nov;62(5):914-9. PubMed PMID: 24019401. Pubmed Central PMCID: 3867444.
31. Knott AB, Perkins G, Schwarzenbacher R, Bossy-Wetzel E. Mitochondrial fragmentation in neurodegeneration. *Nature reviews Neuroscience.* 2008 Jul;9(7):505-18. PubMed PMID: 18568013. Pubmed Central PMCID: 2711514.
32. Guo X, Disatnik MH, Monbureau M, Shamloo M, Mochly-Rosen D, Qi X. Inhibition of mitochondrial fragmentation diminishes Huntington's disease-associated neurodegeneration. *The Journal of clinical investigation.* 2013 Dec;123(12):5371-88. PubMed PMID: 24231356. Pubmed Central PMCID: 3859413.
33. Higgins GC, Coughlan MT. Mitochondrial dysfunction and mitophagy: the beginning and end to diabetic nephropathy? *British journal of pharmacology.* 2014 Apr;171(8):1917-42. PubMed PMID: 24720258. Pubmed Central PMCID: 3976613.
34. Guido C, Whitaker-Menezes D, Lin Z, Pestell RG, Howell A, Zimmers TA, et al. Mitochondrial fission induces glycolytic reprogramming in cancer-associated myofibroblasts, driving stromal lactate production, and early tumor growth. *Oncotarget.* 2012 Aug;3(8):798-810. PubMed PMID: 22878233. Pubmed Central PMCID: 3478457.

Accepted

**Tables**
**Table 1. Phenotypic and metabolic characteristics of rats**

	<b>Body weight (g)</b>	<b>Kidney weight:BW (x10<sup>-3</sup>)</b>	<b>Blood Glucose (mmol/l)</b>	<b>GHb (%)</b>
<b>Control 4 weeks</b>	454±17	6.9±0.3	8.9±1.1	4.4±0.9
<b>Diabetic 4 weeks</b>	319±47*	10.6±0.6*	29.4±4.4*	7.6±1.4*
<b>Control 8 weeks</b>	451±42	6.1±0.3	8.6±1.0	4.1±1.1
<b>Diabetic 8 weeks</b>	295±54*	10.5±1.1*	30.5±5.1	7.8±1.0*
<b>Control 16 weeks</b>	517±56	6.0±1.0	7.6±0.4	4.5±0.2
<b>Diabetic 16 weeks</b>	374±41*	10.5±1.2*	26.6±3.5*	6.6±0.9*
<b>Control 32 weeks</b>	572±30	5.8±0.6	6.9±0.8	4.2±0.9
<b>Diabetic 32 weeks</b>	449±21*	9.9±1.3*	28.2±2.9	7.8±0.7*

Data are mean±SD, *n*=10 per group. BW, body weight; GHb, glycated haemoglobin.  
\**P*<0.0001 vs Control at the same timepoint.

Accepted Manuscript

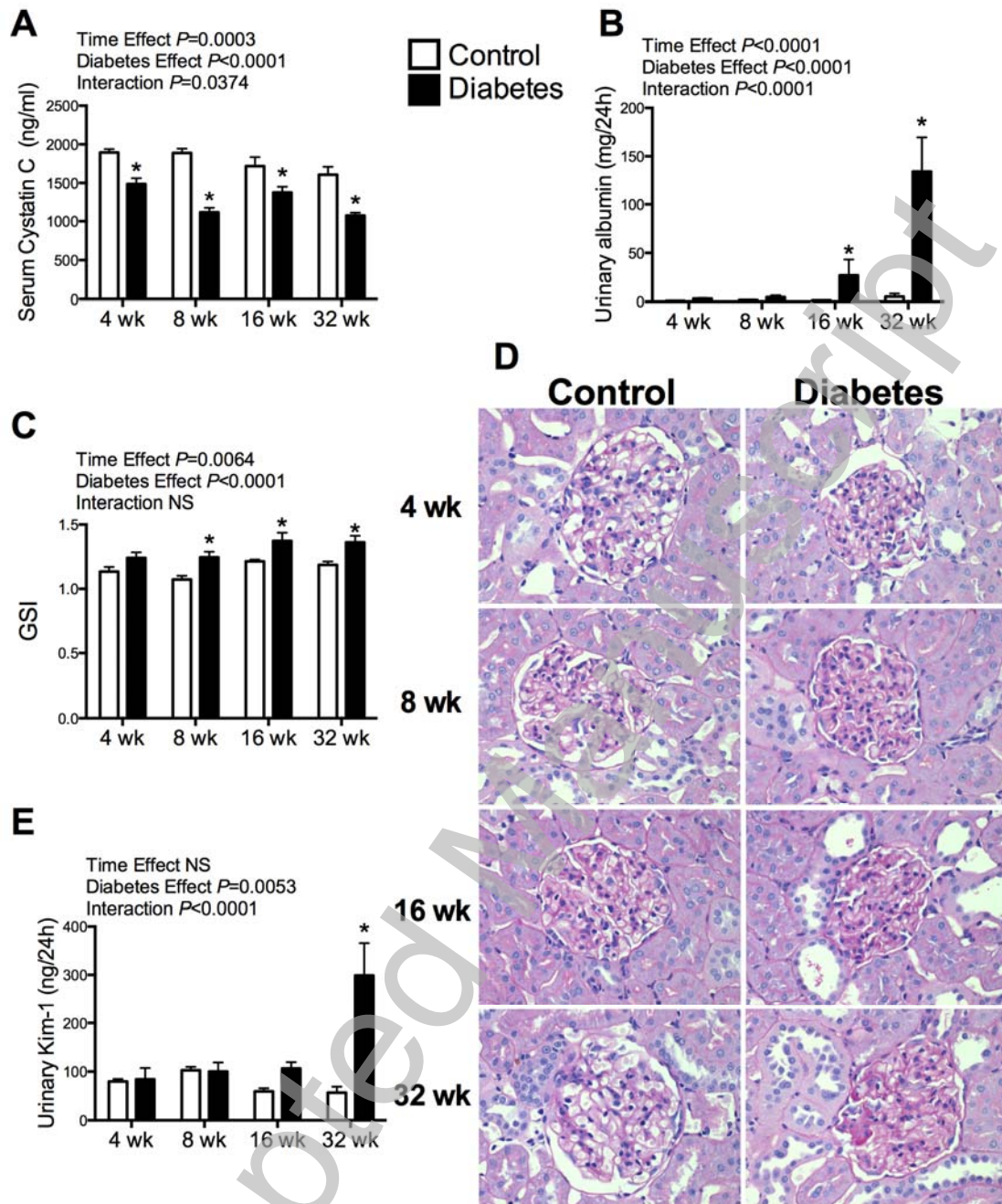


**Figure 1. Tracking development of the renal lesion in diabetic kidney disease.** (A) Serum cystatin C; (B) Urinary albumin excretion; (C) Glomerulosclerotic index (GSI); (D) Photomicrographs of PAS-stained renal cortex, x400 magnification; (E) Urinary excretion of kidney injury molecule-1 (KIM-1). Data are mean $\pm$ SEM,  $n=10$  rats per group. \* $p<0.05$  compared to WT control at the same timepoint.

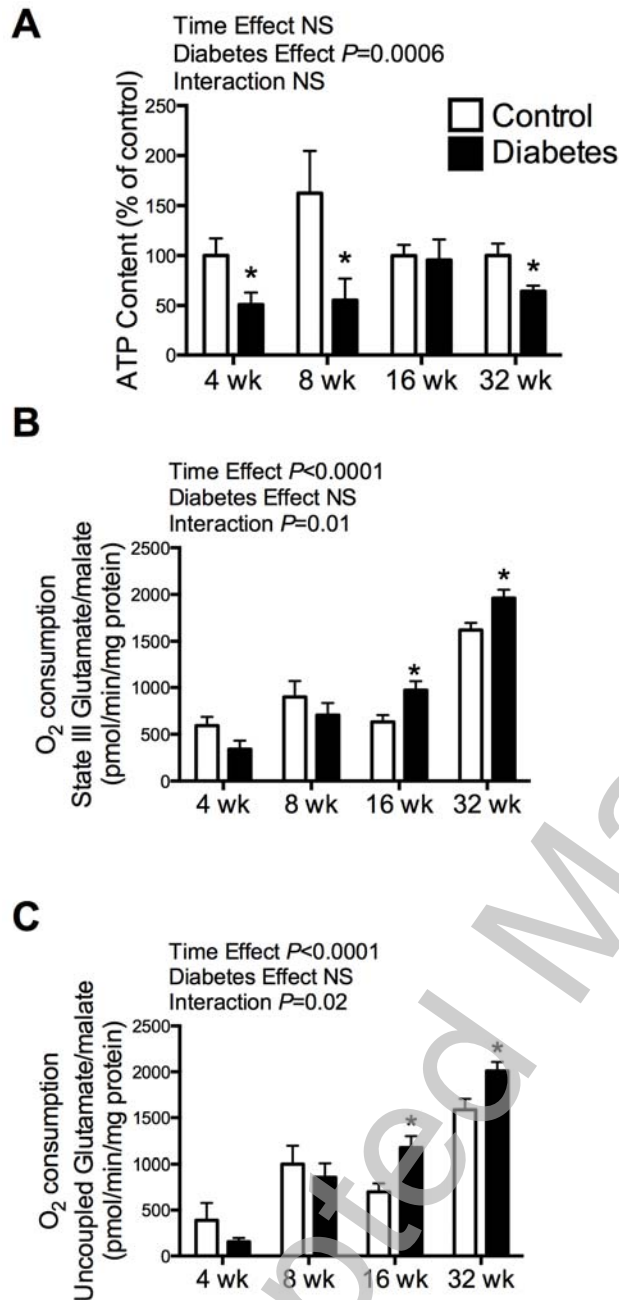


**Figure 2. Changes in mitochondrial bioenergetics precede development of renal structural injury and albuminuria.** Mitochondrial bioenergetics was measured in freshly isolated mitochondria from renal cortex. **(A)** Renal mitochondrial ATP; **(B)** State III Complex I-driven oxygen consumption rate (OCR); **(C)** Uncoupled Complex I-driven OCR. Data are mean $\pm$ SEM,  $n=5$  rats per group. \* $p<0.05$  compared to WT control at the same timepoint.



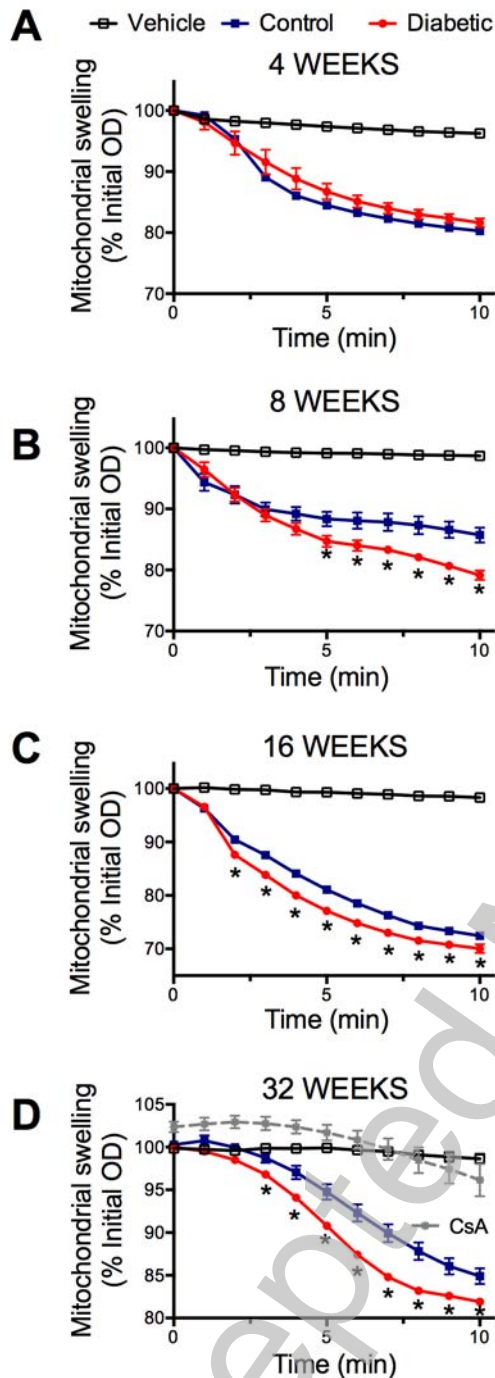


**Figure 3. Increased susceptibility to mitochondrial permeability transition pore opening coincides with the development of renal morphological injury.** Freshly isolated mitochondria from the renal cortex was exposed to vehicle, calcium (to induce pore opening) or calcium plus the mPT pore inhibitor, cyclosporin A, and mPT pore opening (swelling) was assessed by light scattering at 450 nm. Data are expressed as % initial absorbance. Mitochondrial swelling in control vs diabetic at **(A)** 4 weeks, **(B)** 8 weeks **(C)** 16 weeks and **(D)** 32 weeks. Data are mean $\pm$ SEM,  $n=5$  rats per group. \* $p<0.05$  compared to WT control at the same timepoint.



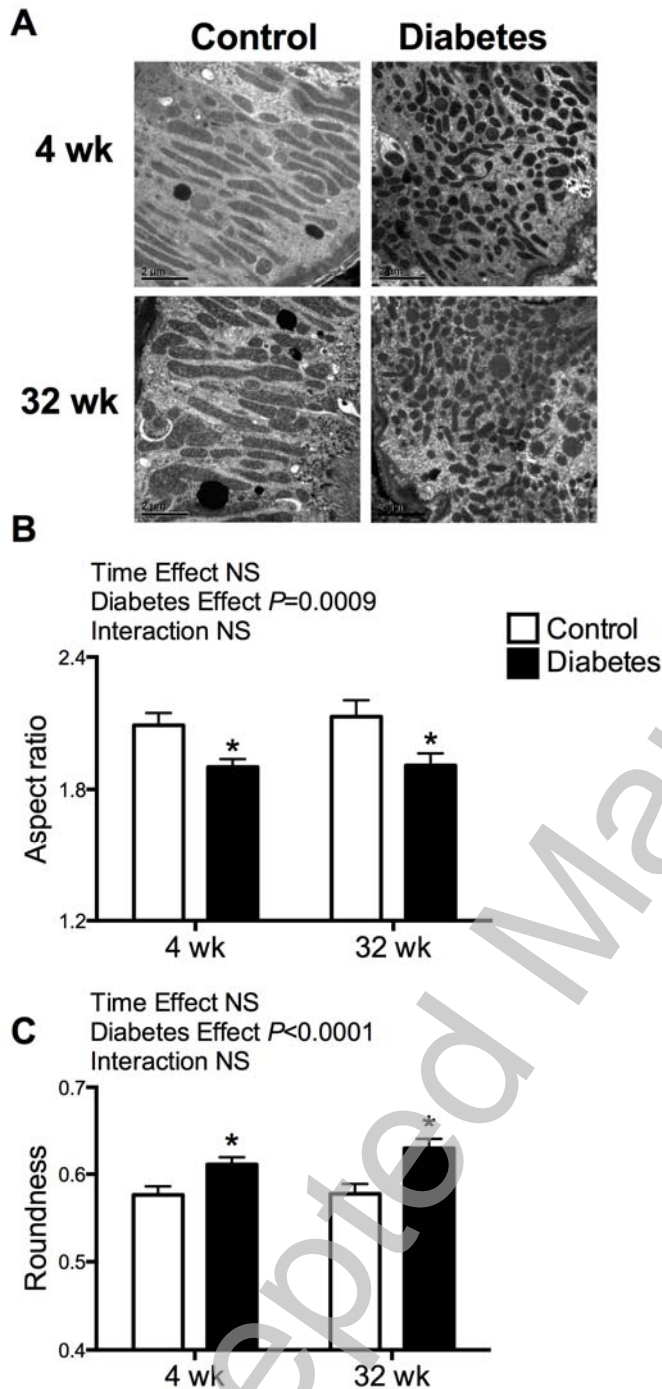


**Figure 4. Proximal tubular cells show mitochondrial fragmentation early in diabetes which persists.** (A) Electron micrographs of renal proximal tubule epithelial cells (PTECs) showing mitochondrial morphology in Control (left) and Diabetic (right) rats at 4 and 32 weeks. x15,000 magnification. Scale bar=2 $\mu$ m. (B) Mitochondrial length and width were measured using ImageJ and aspect ratio was calculated (length/width). (C) Mitochondrial roundness was measured using ImageJ. Data are mean $\pm$ SEM,  $n=10$  images per rat (with between 40 to 200 mitochondria scored in each image),  $n=5$  rats per group.

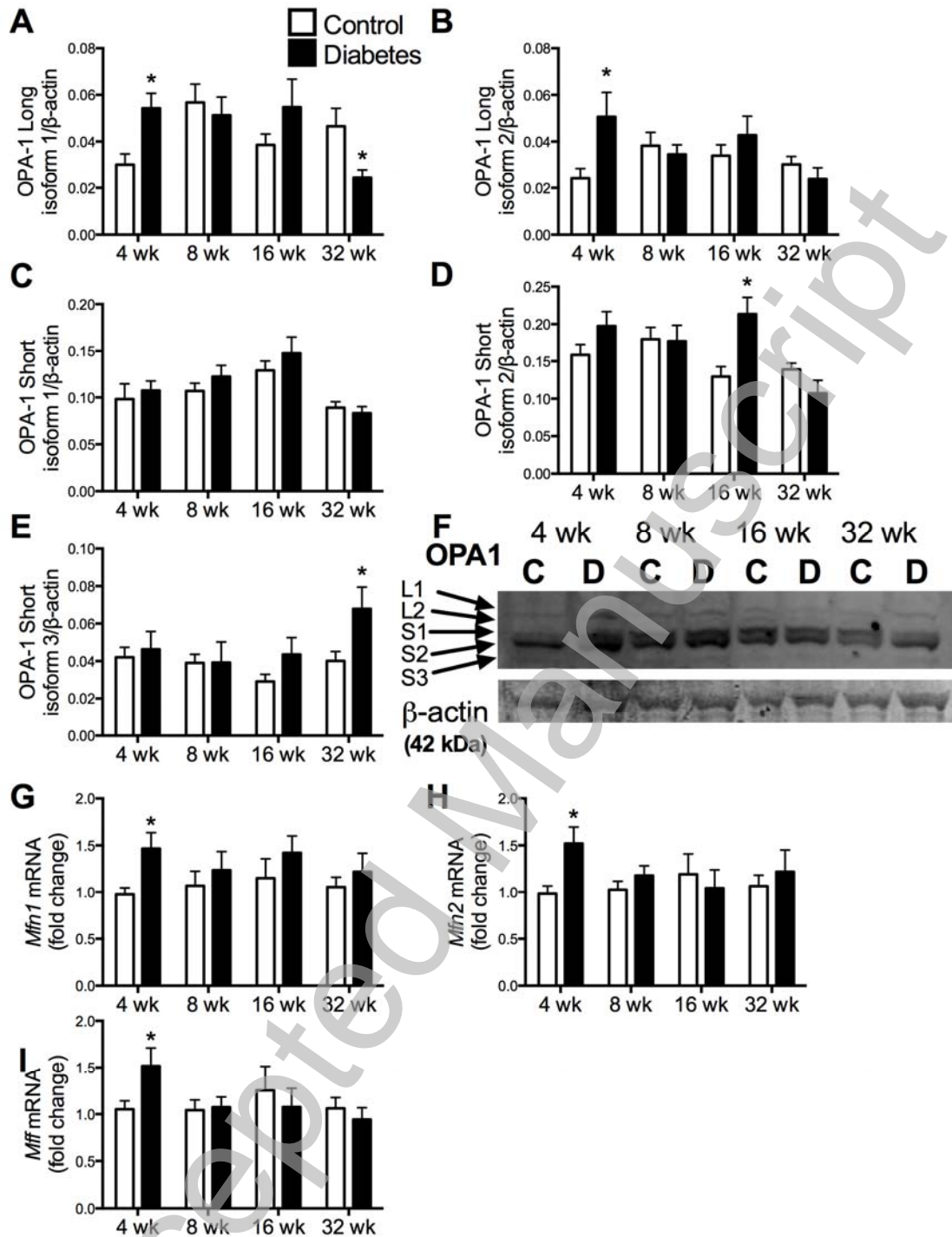


**Figure 5. Proteins involved in mitochondrial fission and fusion are altered throughout the time-course of diabetes.** Quantitation of OPA1 western blot,  $n=6$  rats per group. (A) OPA1 Long isoform 1; (B) OPA1 Long isoform 2; (C) OPA1 Short isoform 1; (D) OPA1 Short isoform 2; (E) OPA1 Short isoform 2. (F) Representative western blot (gradient gel) of OPA1 in showing the five isoforms: long isoforms 1 and 2 (L1 and L2) and short isoforms 1-3 (S1, S2 and S3) (spanning 80-100kDa). Beta actin loading control (42 kDa, bottom). (G-J) Quantitative PCR analysis of genes involved in mitochondrial dynamics in renal cortex (G) Mitofusin (*Mfn*)-1; (H) *Mfn*2; (I) Mitochondrial fission factor (*Mff*),  $n=10$  rats per group.

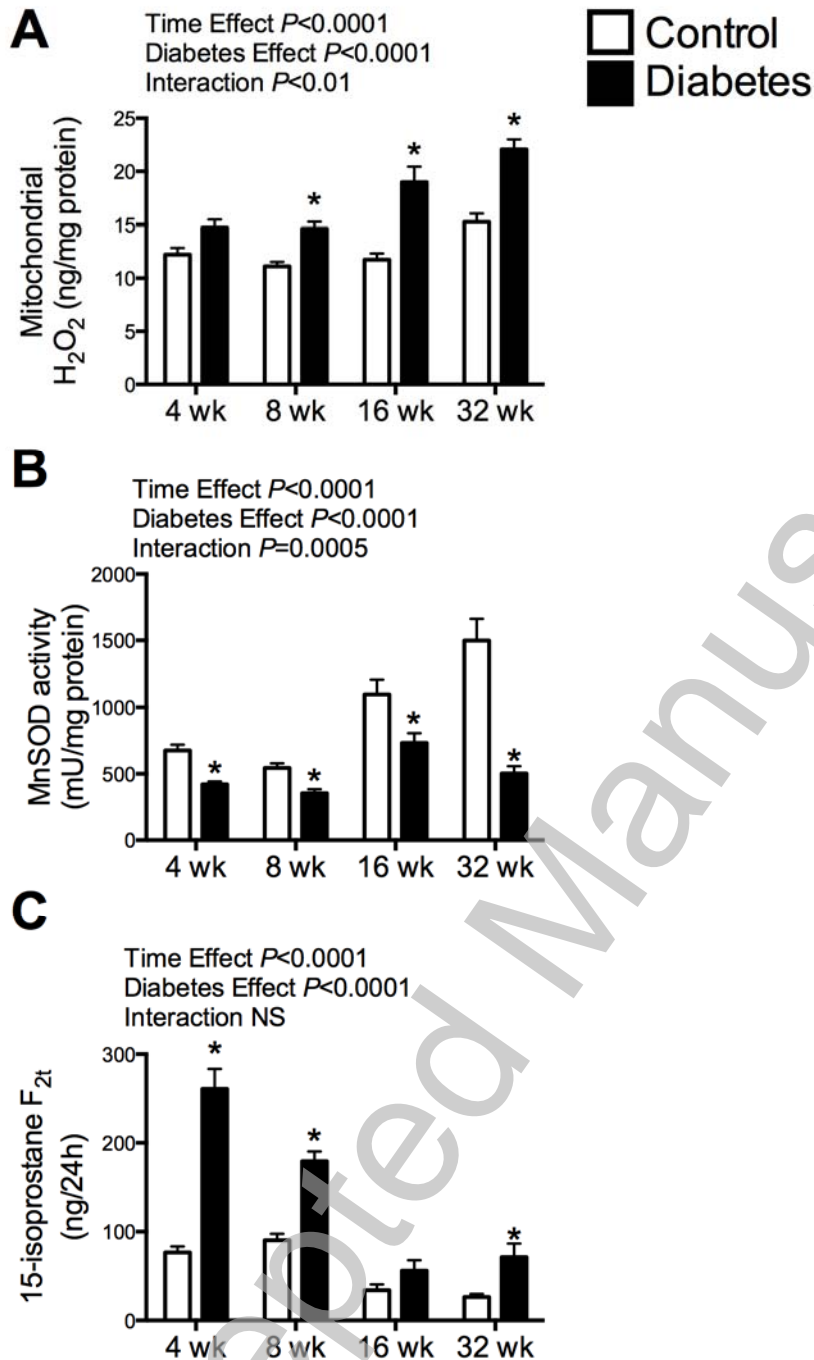


**Figure 6. Oxidative stress response is upregulated in diabetic nephropathy.** (A) Mitochondrial hydrogen peroxide production; (B) Manganese superoxide dismutase activity (MnSOD); (C) Urinary excretion of 15-isoprostane  $F_{2t}$ . Data are mean  $\pm$  SEM,  $n=5-10$  rats per group. \* $p < 0.05$  compared to WT control at the same timepoint.